CrystEngComm

www.rsc.org/crystengcomm

Volume 12 | Number 7 | July 2010 | Pages 1963–2268

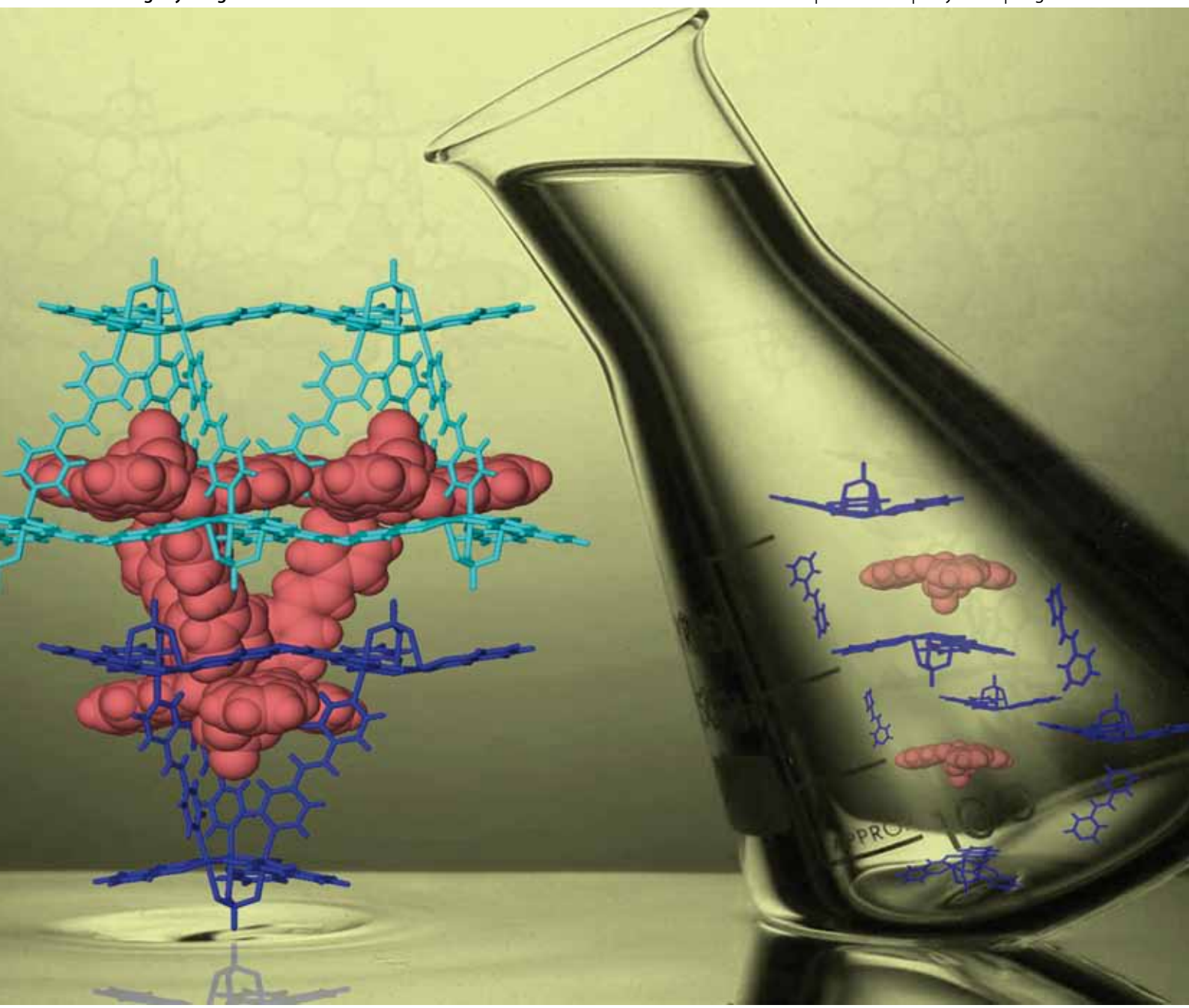

RSC Publishing

PAPER
Papaefstathiou, Brechin *et al.*
Assembling molecular triangles into discrete and infinite architectures

HIGHLIGHT
Levilain and Coquerel
Pitfalls and rewards of preferential crystallization

Assembling molecular triangles into discrete and infinite architectures†

Ross Inglis,[a] Athanassios D. Katsenis,[b] Anna Collins,[a] Fraser White,[a] Constantinos J. Milios,[c] Giannis S. Papaefstathiou*[b] and Euan K. Brechin*[a]

Received 10th February 2010, Accepted 21st April 2010
First published as an Advance Article on the web 7th June 2010
DOI: 10.1039/c002761h

Having established that molecules with general formulae $[Mn^{III}_6O_2(R\text{-sao})_6(O_2CR)_2(L)_{4-6}]$ ($[Mn_6]$) and $[Mn^{III}_3O(R\text{-sao})_3(X)(L)_3]$ ($[Mn_3]$) (saoH$_2$ = salicylaldoxime; R = H, Me, Et *etc*; X = RCO_2^-, ClO_4^-; L = solvent), with the latter being the analogous "half" molecules of the former, exhibit the phenomenon of single-molecule magnetism, we have exploited them as building blocks to construct supramolecular architectures by means of host–guest interactions and coordination driven self-assembly. A number of discrete and infinite architectures, namely $[Mn^{III}_3O(Ph\text{-sao})_3(4Cl\text{-sbz})_3(MeOH)_3]_2(OH)(ClO_4)\cdot 2MeOH$ (**1**·2MeOH), $[Mn^{III}_3O(Ph\text{-sao})_3(4Me\text{-sbz})_3(EtOH)_3]_2(OH)(NO_3)$ (**2**), $\{[Mn^{III}_3O(Et\text{-sao})_3(4,4'\text{-bpy})_2(MeOH)]\ ClO_4\cdot 1.5MeOH\cdot Et_2O\}_n$ (**3**·1.5MeOH·Et$_2$O), $\{[Mn^{III}_3O(sao)_3(4,4'\text{-bpe})_{1.5}]ClO_4\cdot 3MeOH\}_n$ (**4**·3MeOH) and $[\{Mn^{III}_3O(Et\text{-sao})_3(O_2CPh)(EtOH)\}_2\{4,4'\text{-bpe}\}_2]$ (**5**), based on the molecular triangle $[Mn_3]$ and various pyridyl-type ligands (4Cl-sbz = 4-chlorostilbazole, 4Me-sbz 4-methylstilbazole, 4,4′-bpy = 4,4′-bipyridine and 4,4′-bpe = *trans*-1,2-bis(4-pyridyl)ethylene) were obtained and structurally and magnetically characterized.

Introduction

With the realization that crystal packing effects may play an important role in influencing the properties of molecular materials, the field of crystal engineering has enabled scientists to develop an understanding of how intermolecular interactions synergistically work and how to deploy them to evolve new areas of chemical research.[1] For this purpose, two special issues were recently devoted to the crystal engineering of molecular magnetic materials, highlighting the recent developments at the interface of supramolecular chemistry and molecular magnetism.[2]

Although Single-Molecule Magnets (SMMs) are indeed molecules and their properties are of molecular origin, crystal packing effects, which include weak interactions (*e.g.* hydrogen bonding, π···π interactions *etc*), often influence their magnetic response, especially at low temperatures.[3] To this end, we have recently initiated a project to both study crystal packing effects upon SMM behaviour and to attempt to utilize SMMs as building blocks for the construction of supramolecular architectures (*i.e.* polygons, polyhedra) and extended networks (*i.e.* coordination polymers).[4]

We recently demonstrated that certain members of a family of hexanuclear and trinuclear Mn^{III} complexes of general formulae $[Mn^{III}_6O_2(R\text{-sao})_6(O_2CR)_2(L)_{4-6}]$ {hereafter denoted as $[Mn_6]$} and $[Mn^{III}_3O(R\text{-sao})_3(X)(L)_3]$ {hereafter denoted as $[Mn_3]$} (saoH$_2$ = salicylaldoxime; R = H, Me, Et *etc*; X = RCO_2^-, ClO_4^-; L = solvent);[5,6] with the latter being the analogous "half" molecules of the former, exhibit the phenomenon of single-molecule magnetism. We showed in each case that it was possible to significantly increase the ground spin state from $S = 4$ to $S = 12$ in the former and from $S = 2$ to $S = 6$ in the latter, enhancing the effective energy barrier for magnetisation reversal to record levels.[5,6] The origin of the AF → F switch arises from an intra-cluster structural distortion of the molecule induced by the 'twisting' of the (-Mn–N–O-) ring, as evidenced by the significant increases in the Mn–N–O–Mn torsion angles observed when derivatised salicylaldoximes were employed.[5d,6c] The replacement of the axial ligands (*e.g.* ClO_4^- or RCO_2^-) provides an additional/alternative route to influence the magnetic response and that, in combination with the high yields and solution stability of the molecular triangles, enables them to serve as building blocks. Since this system was found to be susceptible to subtle changes around the metal core, we reasoned that it would be possible to further influence their magnetic response by incorporating them into supramolecular architectures by means of host–guest interactions and coordination driven self-assembly.[7]

Taking advantage of the potentially "vacant" coordination axes on each Mn^{III} ion of $[Mn_3]$ we have managed to isolate a series of discrete and infinite assemblies by attaching terminal (4-chlorostilbazole, 4Cl-sbz and 4-methylstilbazole, 4Me-sbz) or bridging (4,4′-bipyridine, 4,4′-bpy and *trans*-1,2-bis(4-pyridyl)-ethylene, 4,4′-bpe) pyridyl-type ligands to them (Scheme 1).

Results and discussion

Syntheses

A typical synthetic procedure for the isolation of a $[Mn_3]$ precursor involves the reaction of one equivalent of a suitable

[a]*School of Chemistry, The University of Edinburgh, West Mains Road, Edinburgh, EH9 3JJ, UK. E-mail: ebrechin@staffmail.ed.ac.uk; Fax: +44 11-275-4598; Tel: +44 131 650 7545*
[b]*Laboratory of Inorganic Chemistry, Department of Chemistry, National and Kapodistrian University of Athens, Panepistimiopolis, 157 71 Zografou, Greece. E-mail: gspapaef@chem.uoa.gr; Fax: +30 210-727-4782; Tel: +30 210-727-4840*
[c]*Department of Chemistry, University of Crete, 71 003 Voutes, Herakleion Crete, Greece*

† CCDC reference numbers 696166 and 696167, 765867–765869. For crystallographic data in CIF or other electronic format see DOI: 10.1039/c002761h

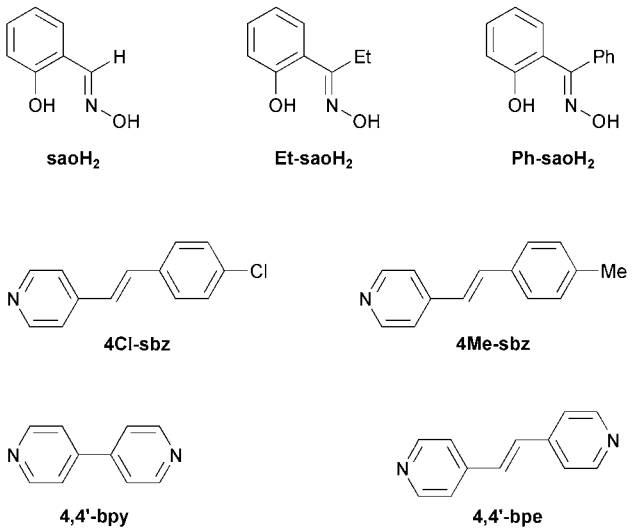

Scheme 1 Ligands discussed in the text.

Mn(II) starting material such as $Mn(ClO_4)\cdot 6H_2O$ with one equivalent of a (substituted) salicylaldoxime (Scheme 1) in alcohol (MeOH or EtOH). The resulting yellowish solution is then treated with base (Et_3N, Et_4NOH, MeONa or $LiOH\cdot H_2O$) to afford a dark green solution from which dark green/black crystals precipitate after slow evaporation. Although dissolution of the $[Mn_3]$ precursor in alcohol or a mixture of alcohol/CH_2Cl_2 and treatment with the terminal or bridging pyridyl ligand affords the desired assembly, we found it more convenient to simply treat the dark green solution obtained by mixing the starting materials with the pyridyl-type ligand in a one-pot reaction. The latter procedure affords the desired assemblies in higher yields than the former. In the case of **5** the $[Mn_6]$ precursor $[Mn^{III}_6O_2(Et\text{-}sao)_6(O_2CPh)_2(EtOH)_4(H_2O)_2]$[5d] was treated with 4,4′-bpe in EtOH to afford the discrete rectangular assembly, while **2** was obtained from the reaction of $Mn(NO_3)_2\cdot 6H_2O$ with Ph-saoH$_2$, Et_3N and 4-Me-sbz in EtOH. See the Experimental section for full details.

Description of structures

For the sake of comparison, the structures of representative $[Mn_3]$ precursors are briefly discussed in terms of describing the structural features that we took under consideration to design the supramolecular assemblies. The representative SMM $[Mn^{III}_3O(Et\text{-}sao)_3(MeOH)_3](ClO_4)$[6c] (Fig. 1) consists of a $[Mn^{III}_3(\mu_3\text{-}O)]^{7+}$ triangular unit with the three $\eta^1{:}\eta^1{:}\eta^1{:}\mu$-Et-sao^{2-} ligands bridging along the edges of the $[Mn_3]$ core. A threefold inversion axis which is perpendicular to the $[Mn_3]$ mean plane passes through the central μ_3-O^{2-}, the perchlorate chlorine atom and one of the ClO_4^- oxygen atoms. A MeOH molecule is attached to each Mn^{III} ion, with all three being oriented on the same (bottom) side of the triangular unit which is further capped by a $\eta^1{:}\eta^1{:}\eta^1{:}\mu_3$ weakly coordinated ClO_4^- anion on the opposite (upper) side. In this arrangement, each Mn^{III} ion adopts a distorted octahedral geometry and displays Jahn–Teller (JT) elongation, as expected for high-spin $3d^4$ ions in near octahedral geometry. The central μ_3-O^{2-} ion deviates by approximately

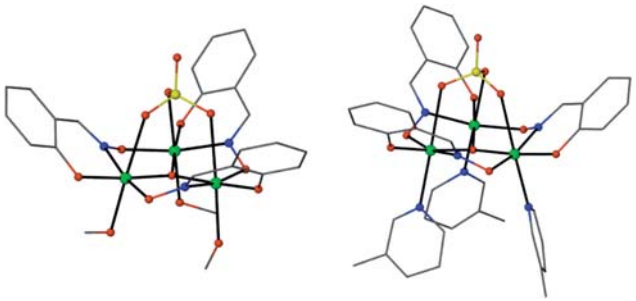

Fig. 1 The molecular structures of $[Mn^{III}_3O(Et\text{-}sao)_3(MeOH)_3](ClO_4)$ and $[Mn^{III}_3O(Et\text{-}sao)_3(\beta\text{-}pic)_3](ClO_4)$. All hydrogen atoms and ethyl groups of the Et-sao^{2-} ligands have been omitted for clarity. Colour code: Mn: green, O: red, N: blue, Cl: yellow, C: grey.

0.18 Å from the $[Mn_3]$ plane towards the terminally bonded MeOH molecules, while the phenyl groups of the Et-sao^{2-} ligands lean toward the perchlorate. The three Mn–N–O–Mn torsion angles are 42.12°. Due to the presence of the capping ClO_4^- anion, the JT axes of the Mn^{III} ions are not parallel and form an angle of ~22.4° to each other and an angle of ~12.96° to the $[Mn_3]$ plane converging towards the ClO_4^- anion. Substitution of the terminally bonded MeOH molecules at the bottom face of the $[Mn_3]$ triangle by substituted pyridine molecules such as β-picoline (β-pic) or 4-ethyl pyridine (4Etpy) does not disturb the metal core or the connectivity of the rest of the ligands resulting in the SMMs $[Mn^{III}_3O(Et\text{-}sao)_3(\beta\text{-}pic)_3](ClO_4)$[6c] (Fig. 1) and $[Mn^{III}_3O(Et\text{-}sao)_3(4Etpy)_3](ClO_4)$.[6c]

Bearing in mind the shape of the $[Mn_3]$ triangles, we reasoned that substitution of the terminally bonded MeOH or pyridine ligands with longer pyridyl-type ligands such as the stilbazoles would create some sort of cavity at the bottom face of the $[Mn_3]$ plane. That came to fruition when 4Cl-sbz was introduced to the methanolic reaction mixture of $Mn(ClO_4)\cdot 6H_2O$/Ph-saoH$_2$/Et_3N from which $[Mn^{III}_3O(Ph\text{-}sao)_3(4Cl\text{-}sbz)_3(MeOH)_3]_2(OH)(ClO_4)\cdot 2MeOH$ (**1**·2MeOH) was obtained.

Complex (**1**) (Table 1, Fig. 2) crystallizes in the rhombohedral space group $R\bar{3}$ and consists of a $[Mn^{III}_3(\mu_3\text{-}O)]^{7+}$ triangular unit with the three Ph-sao^{2-} ligands bridging in a $\eta^1{:}\eta^1{:}\eta^1{:}\mu$ fashion along the edges of the $[Mn_3]$ core. A threefold inversion axis which is perpendicular to the $[Mn_3]$ mean plane passes through the central μ_3-O^{2-} (O111). A 4Cl-sbz molecule is attached to each Mn^{III} ion, with all three being oriented on the same (bottom) side of the $[Mn_3]$ plane which is further capped by three terminal MeOH molecules on the opposite (upper) side instead of the capping ClO_4^- anion found in the precursors, resulting in a cationic $[Mn_3]^+$ complex where all Mn^{III} atoms are in an axially elongated octahedral environment (Fig. 2). The three stilbazole molecules diverge from the bottom of the $[Mn_3]$ triangle toward the outside, creating an open bowl-shaped cavity. Two such $[Mn_3]^+$ complexes have assembled with their bottom faces being parallel and face-to-face having turned by 60° along the three fold axis with respect to each other such that the 4Cl-sbz of one $[Mn_3]^+$ is sitting between two 4Cl-sbz molecules of the other $[Mn_3]^+$. In this [inter-digitated] arrangement, a closed cavity is formed where a disordered ClO_4^- (over two positions with 50% occupancy) is situated, being hydrogen bonded (with 12 H-bonds, 4 unique) to the pyridyl and ethylene hydrogen atoms of

Table 1 Crystallographic data for complexes **1–5**

	1	**2**	**3**	**4**	**5**
Chemical formula	$C_{82}H_{73.5}N_6O_{13.5}Cl_{3.5}Mn_3$	$C_{87}H_{84.5}N_{6.5}O_{12}Mn_3$	$C_{53.5}H_{63}N_7O_{14.5}ClMn_3$	$C_{42}H_{42}N_6O_{14}ClMn_3$	$C_{96}H_{96}N_{10}O_{20}Mn_6$
Formula Mass	1647.91	1577.97	1236.39	1055.09	2039.49
Crystal system	Hexagonal	Hexagonal	Monoclinic	Trigonal	Monoclinic
Space group	$R\bar{3}$	$R\bar{3}$	$C2/c$	$P\bar{3}/c$	$P2_1/n$
a/Å	21.4412(13)	21.4257(4)	27.8361(10)	15.6887(3)	13.4841(4)
b/Å	21.4412(13)	21.4257(4)	15.6707(6)	15.6887(3)	18.4592(5)
c/Å	28.5829(17)	28.5757(6)	30.6046(12)	22.2702(8)	19.6489(6)
α (°)	90.00	90.00	90.00	90	90
β (°)	90.00	90.00	112.593(2)	90	104.358(2)
γ (°)	120.00	120.00	90.00	120	90
V/Å^3	11379.8(12)	11360.5(4)	12325.5(8)	4747.1(2)	4738.0(2)
Z	3	3	2	4	2
Reflections measured	22940	41157	44430	21939	70341
Independent reflections	7686	5184	8852	4188	12809
R_{int}	0.0459	0.0470	0.0543	0.075	0.059
$wR(F^2)$ (all data)[a]	0.1929	0.1385	0.2261	0.1807	0.1737
R_1 ($I > 2\sigma(I)$[b,c]	0.0656	0.0511	0.0877	0.0666	0.0717
GOF on F^2	1.037	1.131	1.099	0.7718	0.9928

[a] $wR2 = [\Sigma w(|F_o^2| - |F_c^2|)^2/\Sigma w|F_o^2|^2]^{1/2}$. [b] For observed data. [c] $R1 = \Sigma||F_o| - |F_c||/\Sigma|F_o|$.

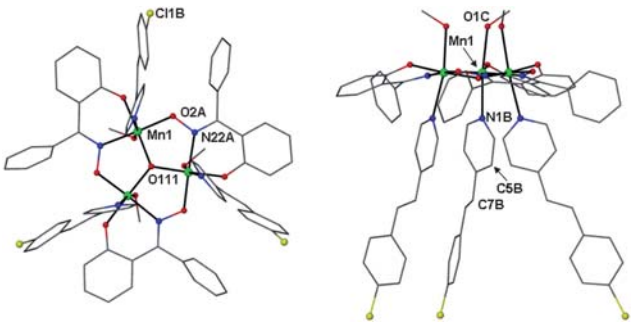

Fig. 2 Top and side views of the $[Mn^{III}_3O(Ph\text{-}sao)_3(4Cl\text{-}sbz)_3(MeOH)_3]^+$ cation in **1**. All hydrogen atoms have been omitted for clarity. Colour code as in Fig. 1.

the 4Cl-sbz ligands (Fig. 3). The $[Mn_3]$ planes within the $\{[Mn_3]\text{-}(ClO_4^-)\text{-}[Mn_3]\}^+$ assembly are separated by 16.151 Å. The $\{[Mn_3]\text{-}(ClO_4^-)\text{-}[Mn_3]\}^+$ units assemble in columns running along c with the upper faces of the $[Mn_3]$ units being face-to-face having a disordered OH^- in between them. The coordination of 4Cl-sbz has disturbed the metal core. The central $\mu_3\text{-}O^{2-}$ ion deviates by ~0.272 Å from the $[Mn_3]$ plane towards the terminally bound 4Cl-sbz ligands, the phenyl groups of the Ph-sao^{2-} now lean toward the 4-chlorostilbazoles (*i.e.* toward the bottom face of the triangle) while the Mn–N–O–Mn torsion angles are reduced to 16.2°.

Complex $[Mn^{III}_3O(Ph\text{-}sao)_3(4Me\text{-}sbz)_3(EtOH)_3]_2(OH)(NO_3)$ (**2**) (Table 1, Fig. 4) also crystallizes in the rhombohedral space group $R\bar{3}$ and consists of a $[Mn^{III}_3(\mu_3\text{-}O)]^{7+}$ triangular unit with the three Ph-sao^{2-} ligands bridging in a $\eta^1{:}\eta^1{:}\eta^1{:}\mu$ fashion along the edges of the $[Mn_3]$ core. It is the nitrate version of complex **1** with three EtOH molecules at the upper side and three 4Me-sbz molecules at the bottom side of the $[Mn_3]$ triangle. The threefold inversion axis passes perpendicular to the $[Mn_3]$ mean plane through the central $\mu_3\text{-}O^{2-}$ (O111). Two $[Mn_3]^+$ units assemble in the same fashion as in **1** to form a cavity which hosts a disordered NO_3^- (over two positions with 50% occupancy), held by 9

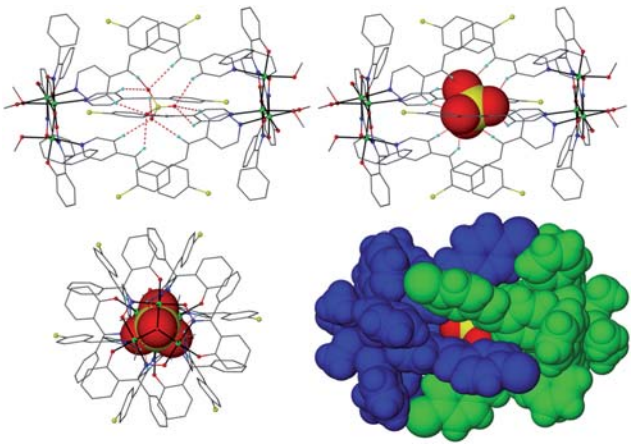

Fig. 3 Perspective views of the $\{[Mn_3]\text{-}(ClO_4^-)\text{-}[Mn_3]\}^+$ assembly found in the crystals of **1**. Most hydrogen atoms have been omitted for clarity. Colour code as in Fig. 1, H: cyan. Bottom right: space filling model of the assembly with the $[Mn_3]^+$ triangles in blue and green.

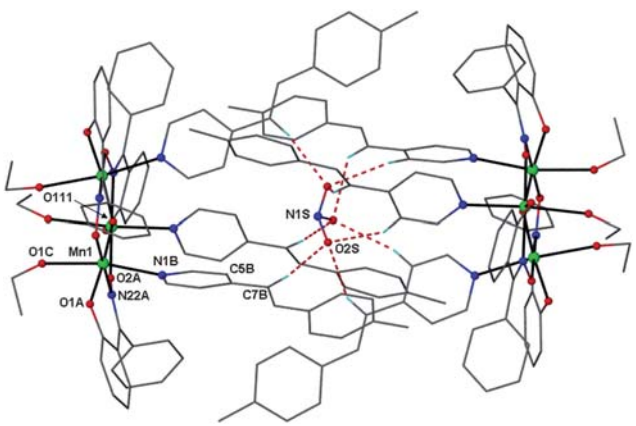

Fig. 4 Perspective view of the $\{[Mn_3]\text{-}(NO_3^-)\text{-}[Mn_3]\}^+$ assembly found in the crystals of **2**. Most hydrogen atoms have been omitted for clarity. Colour code as in Fig. 1, H: cyan.

hydrogen bonds (3 unique) to the pyridyl and ethylene hydrogen atoms of the 4Me-sbz ligands (Fig. 4).

The $[Mn_3]$ planes within the $\{[Mn_3]\text{-}(NO_3^-)\text{-}[Mn_3]\}^+$ assembly are again parallel but the distance between them is reduced to 15.833 Å due to the presence of the smaller nitrate ion in the cavity. A disordered OH^- is situated between the $\{[Mn_3]\text{-}(NO_3^-)\text{-}[Mn_3]\}^+$ units which also assemble in columns along *c* (Fig. 5). The central $\mu_3\text{-}O^{2-}$ ion deviates by ~0.275 Å from the $[Mn_3]$ plane towards the 4Me-sbz ligands, the phenyl groups of the Ph-sao^{2-} lean toward the 4Me-sbz, while the Mn–N–O–Mn torsion angles are further reduced to 13.4°. Complexes **1** and **2** are rare examples of polynuclear metal complexes that have assembled not by coordination bonds[8] but by weak host–guest interactions to create a cavity that clathrates a counter anion by C–H···O interactions.[9]

Aiming to create an extended network by assembling the molecular triangles, we employed 4,4′-bipyridine (4,4′-bpy) in the methanolic reaction mixture of $Mn(ClO_4)\cdot 6H_2O$/Et-saoH$_2$/MeONa from which $\{[Mn^{III}_3O(Et\text{-}sao)_3(4,4'\text{-}bpy)_2(MeOH)]\text{-}ClO_4\cdot 1.5MeOH\cdot Et_2O\}_n$ (**3**·1.5MeOH·Et$_2$O) was obtained after Et$_2$O diffusion. Complex **3** (Table 1, Fig. 6) crystallizes in the monoclinic space group *C*2/*c* and consists of a $[Mn^{III}_3(\mu_3\text{-}O)]^{7+}$ triangular unit with the three $\eta^1{:}\eta^1{:}\eta^1{:}\mu$-Et-sao^{2-} ligands bridging along the edges of the $[Mn_3]$ core and the central $\mu_3\text{-}O^{2-}$ ion (O123) deviating only ~0.015 Å from the $[Mn_3]$ plane. The Mn–N–O–Mn torsion angles are 28.41° for Mn1–N–O–Mn3, 12.79° for Mn3–N–O–Mn2 and 14.92° for Mn2–N–O–Mn1. The $[Mn_3]$ triangles and the 4,4′-bpy ligands have assembled to create a ladder-like one dimensional polymer with two 4,4′-bpy molecules bridging between the $[Mn_3]$ units (Fig. 6). In this arrangement, Mn1 is in an axially elongated octahedral environment with two pyridyl$_{4,4'\text{-bpy}}$ nitrogen atoms at the axial positions, Mn2 is in a square pyramidal environment with a pyridyl$_{4,4'\text{-bpy}}$ nitrogen atom at the axial position and Mn3 is in an axially elongated octahedral environment with a methanol oxygen atom and a pyridyl$_{4,4'\text{-bpy}}$ nitrogen atom at the axial positions.

A careful inspection of the $\{\text{-}[Mn_3]\text{-}(4,4'\text{-bpy})_2\text{-}[Mn_3]\text{-}\}_n$ chain reveals that Mn1 is connected (through a 4,4′-bpy) to a Mn2 on its right and to a Mn3 on its left (Fig. 6). This arrangement dictates that the $[Mn_3]$ core turns around along the polymer axis and this in turn creates a four component repeating unit $([Mn_3]_4)_n$ as shown in Fig. 7. Every two $[Mn_3]$ planes within the four component repeating unit are parallel (*i.e.* plane 1 ‖ plane 2 and plane 3 ‖ plane 4 in Fig. 7) and separated by 11.228 Å, while the distance between the central $\mu_3\text{-}O^{2-}$ of planes 2 and 3 is 12.145 Å. The two sets of parallel planes form an angle of 19.03°.

In order to further exploit the ability of the $[Mn_3]$ triangles to form polymeric structures we employed the longer bis-pyridyl ligand *trans*-1,2-bis(4-pyridyl)ethylene (4,4′-bpe) into a methanolic reaction mixture of $Mn(ClO_4)_2\cdot 6H_2O$ and saoH$_2$. Dark green crystals of $\{[Mn^{III}_3O(sao)_3(4,4'\text{-bpe})_{1.5}]ClO_4\cdot 3MeOH\}_n$ (**4**·3MeOH) were obtained after slow evaporation of the solution. Complex **4** (Table 1, Fig. 8) crystallizes in the trigonal space group $P\bar{3}/c$ and consists of $\mu_3\text{-}O^{2-}$ centered $[Mn^{III}_3O(sao)_3]ClO_4$ units and 4,4′-bpe molecules.

The components have assembled to form a 2D coordination polymer (Fig. 9) where the 4,4′-bpe molecules bridge the $[Mn_3]$ units. Three $\eta^1{:}\eta^1{:}\eta^1{:}\mu$-sao^{2-} ligands and a capping ClO_4^- anion surround the $[Mn_3]$ unit in **4**. A threefold axis passes through the central $\mu_3\text{-}O^{2-}$ (O2), the ClO_4^- chlorine atom (Cl20) and one of the perchlorate oxygen atoms (O22) and is perpendicular to the $[Mn_3]$ plane. The Mn^{III} ions are in axially elongated octahedral

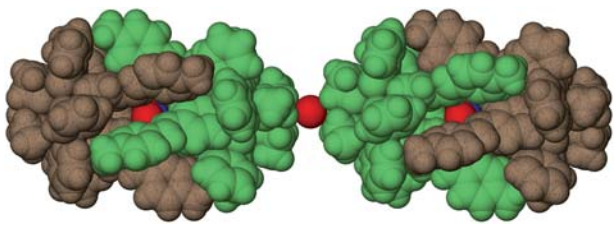

Fig. 5 The $\{[Mn_3]\text{-}(NO_3^-)\text{-}[Mn_3]\}(OH)$ columns in **2** along *c*. Similar packing is observed in $\{[Mn_3]\text{-}(ClO_4^-)\text{-}[Mn_3]\}(OH)$ of **1**.

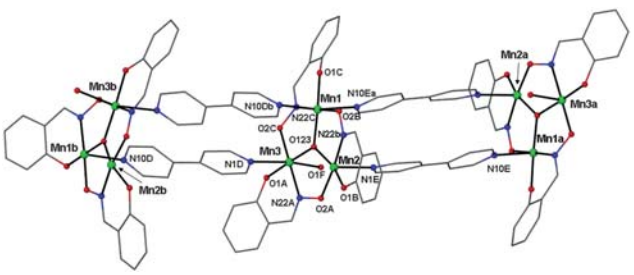

Fig. 6 View of the polymeric chain of **3**. Colour code as in Fig. 1. Symmetry codes: a: ½−x, 3/2−y, b: −z; −x, y, ½−z.

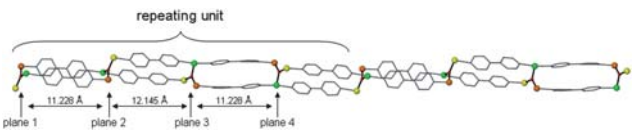

Fig. 7 The four component repeating unit found in **3**. Colour code: Mn1: green, Mn2: orange, Mn3: yellow, O: red.

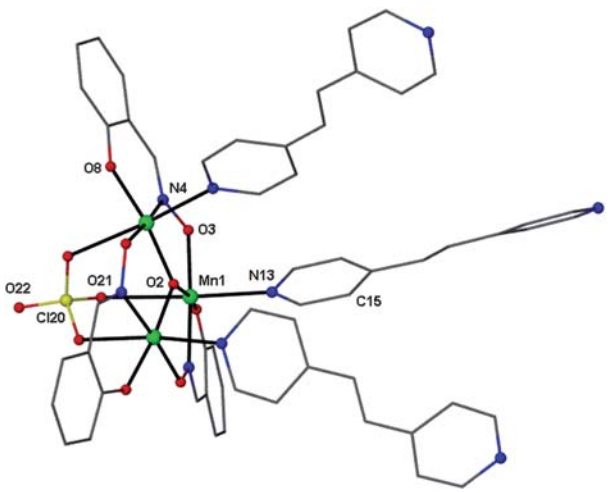

Fig. 8 The molecular structure of the triangle in **4**. All hydrogen atoms have been omitted for clarity. Colour code as in Fig. 1.

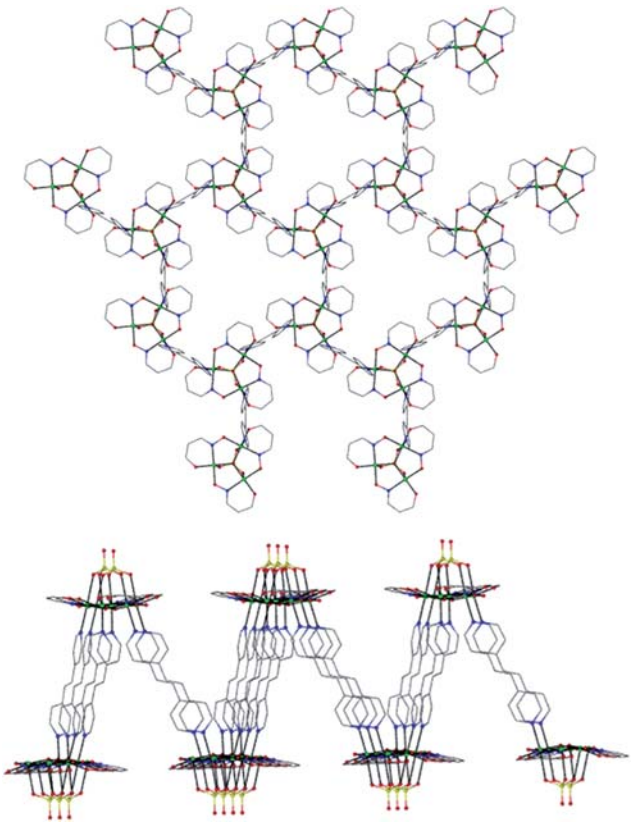

Fig. 9 Top and side views of the 2D (6,3)-net of **4**. All hydrogen atoms and most of the carbon atoms of the sao^{2-} ligands have been omitted for clarity. Colour code as in Fig. 1.

environments with the JT axes [O21–Mn1–N13] converging towards the ClO_4^- side as seen in the precursor triangles $[Mn^{III}_3O(Et\text{-}sao)_3(MeOH)_3](ClO_4)$ and $[Mn^{III}_3O(Et\text{-}sao)_3(\beta\text{-}pic)_3](ClO_4)$. A 4,4′-bpe molecule is attached to each Mn^{III} ion, with all three being oriented on the same (bottom) side of the $[Mn_3]$ plane. The central μ_3-O^{2-} ion deviates by 0.303 Å from the $[Mn_3]$ plane toward the 4,4′-bpe molecules while the Mn–N–O–Mn torsion angles have increased to 17.27° in comparison to those in **1** and **2**, but are still much smaller than those found in the precursor $[Mn^{III}_3O(Et\text{-}sao)_3(MeOH)_3](ClO_4)$.

The 2D network adopted by **4** conforms to a (6,3) regular net with the $[Mn_3]$ units acting as three-connected nodes (Fig. 9). Due to the peculiar shape of the $[Mn_3]$ unit which is non-planar and the orientation of the connection sites on the $[Mn_3]$ cluster which are all pointing toward the same side of the $[Mn_3]$ plane and converging towards the ClO_4^- side, the 2D network is highly distorted such that the $[Mn_3]$ units are placed alternately above and below the mean plane of the 2D net. This arrangement gives rise to the formation of conical cavities within the body of the 2D framework which are approximately 12.6 Å thick (Fig. 9). The upper rims of the conical cavities are pointing alternately above and below the plane of the net such that half of the rims of the cavities point above and half below the layer. Each cavity is composed of a $[Mn_3]$ unit, which serves as the bottom of the cavity and three 4,4′-bpe molecules, while three other $[Mn_3]$ units from the same net are attached to each of the three 4,4′-bpe molecules narrowing the "gates" of the cavities' rims.

A salient feature of the structure of **4** is that the size of each $\{[Mn_3](4,4'\text{-bpe})_3[Mn_3]_3\}$ cavity is large enough to host a $[Mn_3]$ unit of an adjacent net (Fig. 10 and 11). This host–guest interaction is further supported by three hydrogen-bonding interactions that involve one of the pyridyl C–H groups of the three cavity-forming 4,4′-bpe molecules and the uncoordinated oxygen atom of the ClO_4^- that caps the $[Mn_3]$ guest [one unique: C15–H151···O22 = 3.363 Å]. The $[Mn_3]$ guest is in an eclipse orientation with respect to the $[Mn_3]$ at the bottom of the host cavity while the three $[Mn_3]$ units at the rim's gate of the conical cavity prohibit the $[Mn_3]$ guest from exiting (Fig. 10). Therefore, each $[Mn_3]$ serves as (i) the bottom for the conical cavity, (ii) one of the gate-keepers of a neighbouring cavity while (iii) acting as the guest for a cavity belonging to a neighbouring net.

Each layer is interlocked with two other layers, one above and one below the middle layer's plane, resulting in an entangled array with an increased dimensionality (*i.e.* from 2D to 3D) (Fig. 12). This interlocking is purely supramolecular in nature since it is based on host–guest and hydrogen bonding interactions as described above. Each layer acts as a host and at the same time as a guest to both neighbouring layers. In principle the layers of **4** could be disentangled by stretching out, but that is prohibited since it is impossible to have the 4,4′-bpe molecules and the $[Mn_3]$ units in the same plane due to the orientation of the connection sites on the $[Mn_3]$ units. From the topological point of view, the interlocking of the 2D layers of **4** does not belong to any known type of entanglement.[10–12] Topological entanglement (*i.e.* interpenetration and polycatenation) is easily excluded since (i) the dimensionality in **4** increases due to the entanglement, (ii) no bond-breaking is required to disentangle the layers, thus excluding interpenetration[11] and (ii) the closed circuits [*i.e.* the hexagonal rings of the (6,3) net of **4**] are not

Fig. 10 Side (left) and top (right) views of the $[Mn_3] \subset \{Mn_3](4,4'\text{-bpe})_3[Mn_3]_3\}$ in **4**.

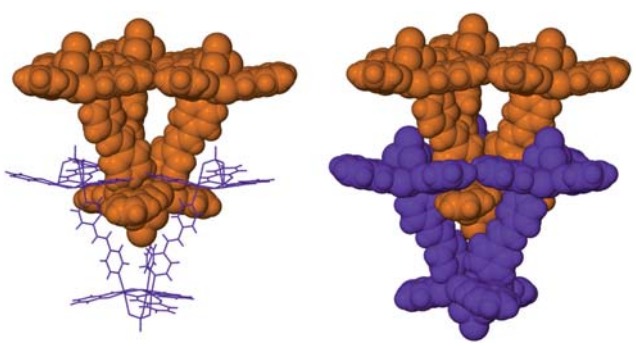

Fig. 11 Views of conical "ice-cream cone" within "an ice-cream cone" units in **4**.

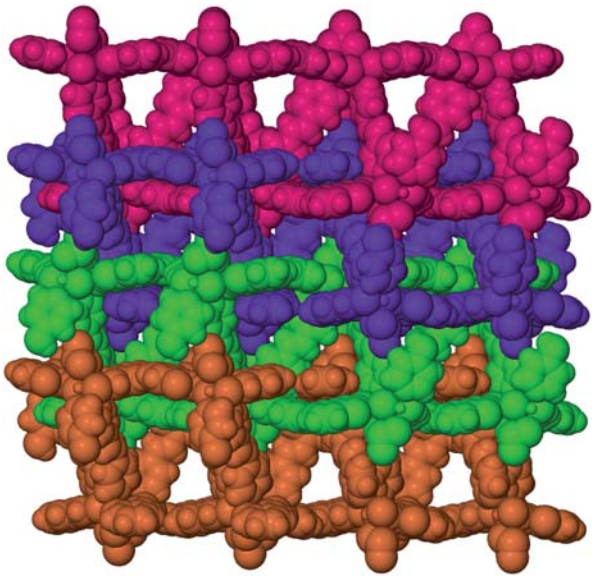

Fig. 12 View of four entangled layers in the crystal of **4**.

catenated (*i.e.* do not form Hopf or Borromean links), thus excluding polycatenation.[12] Euclidean entanglement[10] (*i.e.* polythreading) can also be excluded since none of the closed loops [*i.e.* the hexagonal circuits of the (6,3) net of **4**] are threaded.

That the layers of **4** form cavities to host the [Mn_3] units of neighbouring layers resulting in an architecture of increased dimensionality means that this is a new type of supramolecular entanglement where real host–guest interactions are responsible for the interlocking.

The next step was to employ a [Mn_6] SMM instead of a [Mn_3] as a precursor. For this purpose, [$Mn^{III}_6O_2$(Et-sao)$_6$(O_2CPh)$_2$(EtOH)$_4$(H_2O)$_2$] was treated with 4,4-bpe in EtOH to produce dark green crystals of [{Mn^{III}_3O(Et-sao)$_3$(O_2CPh)(EtOH)}$_2${4,4′-bpe}$_2$] (**5**). Complex **5** (Table 1, Fig. 13) crystallizes in the monoclinic space group $P2_1/n$ and consists of two [$Mn^{III}_3(\mu_3\text{-O})]^{7+}$ triangular units with the three $\eta^1{:}\eta^1{:}\eta^1{:}\mu$-Et-sao^{2-} ligands bridging along the edges of the [Mn_3] core and two 4,4′-bpe molecules bridging the [Mn_3] triangles. An inversion centre in the middle of the molecule correlates the two [Mn_3] units. The two 4,4′-bpe molecules are organized between the two [Mn_3] clusters in a face-to-face stacked arrangement and separated by 3.5 Å. Two phenyl groups of two Et-sao^{2-} ligands are twisted towards the 4,4′-bpe side with the third pointing in the opposite direction. Two of the three Mn^{III} ions are in distorted octahedral environments with the third adopting a square pyramidal geometry. The capping μ_3-ClO_4^- in **4** and in the [Mn_3] precursors has been replaced by a *syn*,*syn* μ-$PhCO_2^-$ and a terminal EtOH molecule.

The ligation of the $PhCO_2^-$ and the EtOH molecules has destroyed the three fold rotation axis present in **1**, **2** and the three fold axis in **4**, thus releasing the JT axes on the Mn^{III} ions from converging towards the same side of the [Mn_3] plane. The Mn^{III} ions that coordinate to the 4,4′-bpe molecules are those in the octahedral environment, with the oxygen atoms from a $PhCO_2^-$ and an EtOH molecule on the apical positions opposite the nitrogen atoms (N4 and N5) of the 4,4′-bpe molecules. The JT axes on those Mn^{III} ions are inclined to each other at an angle of 19.13° [O10–Mn1N5 ∠ O8–Mn3–N4], and are thus more twisted than the analogous axes in their [Mn_3] precursors, **1**, **2** and **4**, although they do not converge towards the $PhCO_2^-$ and the EtOH ligands. The central μ_3-O^{2-} ion deviates by 0.274 Å from the [Mn_3] plane toward the 4,4′-bpe molecules. The Mn–N–O–Mn torsion angles are 24.17° for Mn1–N–O–Mn2, 10.62° for Mn2–N–O–Mn3 and 42.73° for Mn32–N–O–Mn1. The replacement of the ClO_4^- ligands by a $PhCO_2^-$ and the EtOH molecule in **5** has lowered the local symmetry around the [Mn_3] cluster giving rise to a polygon (*i.e.* a rectangle) instead of a coordination polymer as in **3** and **4**. Alternatively, **5** might be described as a "dimer of clusters" or a "pair of clusters"[4e,13] which is a rather new perspective of looking at how magnetic clusters can be arranged in the crystal lattice with respect to each other.[14]

Magnetism

Dc magnetic susceptibility studies were carried out on powdered crystalline samples of **1–5** in the temperature range 5–300 K in a field of 0.1 T. The $\chi_M T$ *vs.* T data for **2**, **3** and **5** are plotted in Fig. 14 with their simulations (solid lines). The data for complexes **1** and **4** have been omitted as they are essentially identical to **2** and **5**, respectively. Room-temperature $\chi_M T$ values

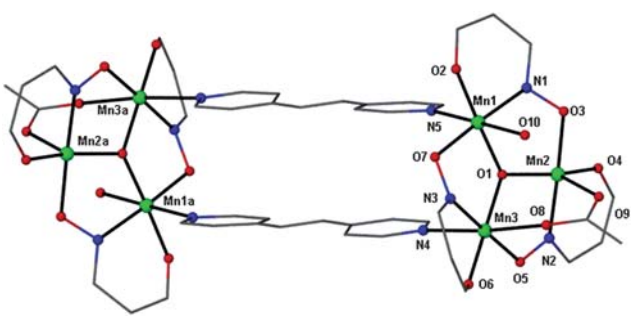

Fig. 13 The rectangular hexanuclear assembly of **5**. All hydrogen and some carbon atoms have been removed for clarity. Colour code as in Fig. 1. Symmetry code: a: −x, 1−y, −z.

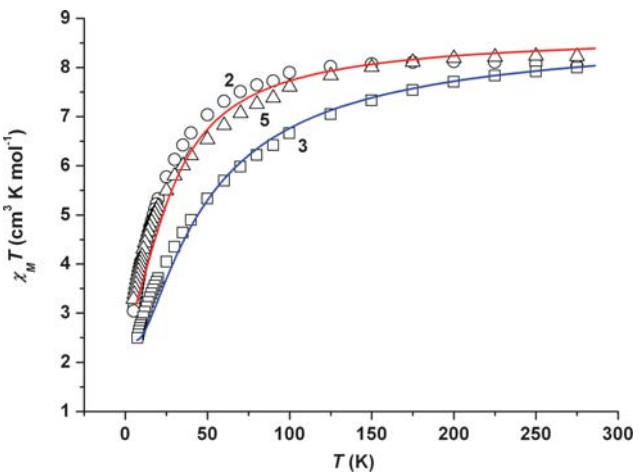

Fig. 14 $\chi_M T$ *vs.* T plots for complexes **2** (○), **3** (□) and **5** (△). The solid lines represent simulations of the experimental data—see the text for details.

for all complexes range from 7.99 to 8.22 cm^3 K mol^{-1}, lower than the expected spin-only ($g = 2$) value for three non-interacting Mn^{III} centres of 9 cm^3 K mol^{-1}, suggesting the presence of dominant antiferromagnetic exchange. In all cases the $\chi_M T$ values decrease gradually as temperature is decreased until approximately 150 K where they drop more rapidly to values between 2.09 and 3.28 cm^3 K mol^{-1} at 5 K.

Complex **3** was successfully simulated[15] employing the Hamiltonian of eqn (1) describing the *2-J* model (isosceles triangle) shown in Scheme 2, giving a ground state $S = 2$ and the parameters $g = 1.98$, $J_1 = -2.80$ and $J_2 = -0.80$ cm^{-1}, with the first excited state ($S = 1$) 4.80 cm^{-1} above the ground state.

Complex **5** was successfully simulated using the *3-J* model (scalene triangle) of eqn (2) [Scheme 2], affording a ground state $S = 2$ and the parameters $g = 1.97$, $J_1 = -1.30$, $J_2 = -2.80$ and $J_3 = 1.20$ cm^{-1}, with the first excited state ($S = 3$) 11.81 cm^{-1} above the ground state. The isosceles *versus* scalene triangle models were employed based on the symmetry of the [Mn_3] unit and the number of significantly different Mn–N–O–Mn torsion angles.

$$\hat{H} = -2J_1\,(\hat{S}_1\cdot\hat{S}_2 + \hat{S}_2\cdot\hat{S}_3) - 2J_2\,(\hat{S}_1\cdot\hat{S}_3) \quad (1)$$

$$\hat{H} = -2J_1\,(\hat{S}_1\cdot\hat{S}_2) - 2\,J_2\,(\hat{S}_2\cdot\hat{S}_3) - 2J_3\,(\hat{S}_1\cdot\hat{S}_3) \quad (2)$$

Complex **2** has crystallographically imposed three-fold symmetry and its susceptibility data could not be reproduced satisfactorily. $S = 2$ is not the anticipated ground state for an antiferromagnetic triangle that possesses idealized three-fold symmetry [an equilateral triangle with the same J across all three exchange pathways). In fact, one expects a singlet, $S = 0$, ground state due to the frustration inherent in the topology. Our previous studies of isolated (molecular) [Mn_3] triangles have only been successful for those molecules in which the frustration has been relieved, *i.e.* the most distorted complexes.[6c] Indeed only two examples of low-spin [Mn_3] complexes from a very large family of molecules, have yielded any useful information—even from single crystal EPR.[6c] The presence of weak exchange comparable in magnitude to d_{ion} results in considerable spin-state mixing, making S ill-defined.

Conclusions

Our adventures in assembling molecular triangles, $[Mn^{III}_3O(R\text{-}sao)_3]^+$, have resulted in a series of discrete and infinite supramolecular architectures featuring self-assembled dimers of triangles that have assembled not by coordination bonds but by weak host–guest interactions to create a cavity that clathrates a counter anion (*i.e.* ClO_4^- and NO_3^-) by C–H···O interactions, a 1D coordination polymer in which the repeating unit is different than the asymmetric unit,[16] a 2D coordination polymer that exhibits a novel type of a supramolecular entanglement which is based on host–guest interactions and increases the dimensionality of the bulk material to 3D and a polygon. The construction of the polygon was rationalized in terms of changing the capping ClO_4^-, that forces the connection coordination axes on each Mn^{III} ion of the [Mn_3] precursor to converge towards its side, to a $PhCO_2^-$ and an EtOH molecule that lower the local symmetry around the [Mn_3], releasing the JT connection axes and therefore directing the self-assembly process. The [Mn_3] core has proved its self stable enough to maintain its integrity upon reaction with various pyridyl ligands and at the same time adaptable to changes by altering its local symmetry. Although these characteristics proved fruitful/compelling for the construction of the supramolecular architectures, they also proved disadvantageous for the construction of magnetic materials since the changes in the magnetic core dramatically reduced the Mn–N–O–Mn torsion angles resulting in materials with small spin ground states. In other words, the use of long pyridyl-type ligands has the effect of flattening the triangular building blocks and thus promoting AF exchange through the oximate bridges affording [Mn_3] units with $S = 2$ ground states. We further exploited the possibility of utilizing the [Mn_3] and [Mn_6] as building blocks for the construction of discrete or infinite architectures by employing polycarboxylate ligands and/or mixed pyridyl/carboxylate ligands.

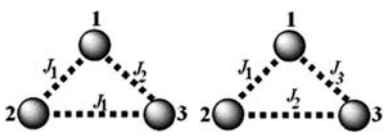

Scheme 2 Schematic detailing the *2−J* (isosceles triangle) and *3−J* (scalene triangle) models employed to simulate the experimental data for **3** and **5**, respectively. The different coupling constants (J_1–J_3) represent exchange between metal ions *via* significantly different Mn–N–O–Mn torsion angles.

Experimental

Materials and methods

All manipulations were performed under aerobic conditions, using materials as received. **CAUTION!** Although no problems were encountered in this work, care should be taken when using the potentially explosive perchlorate anion. Substituted salicylaldoximes[17] and stilbazoles[18] were synthesized following known procedures. The syntheses, structures and magnetic properties of the [Mn_3] and [Mn_6] precursors have already been reported.[5,6] The syntheses of complexes **4** and **5** have been communicated.[4a] Variable-temperature, solid-state direct current (dc) magnetic susceptibility data down to 1.8 K were collected on a Quantum Design MPMS-XL SQUID magnetometer equipped with a 7 T dc magnet. Diamagnetic corrections were applied to the observed paramagnetic susceptibilities using Pascal's constants.

X-ray crystallography

Diffraction data were collected at 150 K on a Bruker Smart Apex CCDC diffractometer, equipped with an Oxford Cryosystems LT device, using Mo radiation. See CIF files and Table 1 for full details.

Synthesis

General synthetic strategies. The supramolecular architectures reported here may be obtained using two synthetic procedures. The first involves the reaction of an appropriate Mn^{II} salt with a (substituted) salicylaldoxime and a base (Et_3N, Et_4NOH, MeONa or $LiOH\cdot H_2O$) in alcohol (MeOH or EtOH) to afford a dark green solution into which either solid or a CH_2Cl_2

solution of the pyridyl ligand was added resulting in the desired assemblies. The second procedure involves the synthesis and isolation of a precursor [Mn_3] triangle (or [Mn_6] in the case of **5**) followed by dissolution in alcohol (MeOH or EtOH) or in a mixture of alcohol/CH_2Cl_2 and addition of solid or a CH_2Cl_2 solution of the pyridyl ligand. Synthetic details are given below for the synthetic procedures which result in the highest yields.

$[Mn^{III}_3O(Ph\text{-}sao)_3(4Cl\text{-}sbz)_3(MeOH)_3]_2(OH)(ClO_4)\cdot 2MeOH$ (**1**·2MeOH)

$Mn(ClO_4)_2\cdot 6H_2O$ (362 mg, 1 mmol), Ph-saoH_2 (213 mg, 1 mmol) and NEt_4OH (1M aqueous solution, 0.5 ml) in MeOH (25 ml) were allowed to stir for 45 min at room temperature. To the resulting dark green solution 4Cl-sbz (216 mg, 1 mmol) was added followed by paper filtration. The solution was left undisturbed to slowly evaporate at room temperature. X-ray quality dark green crystals of **1** were obtained in 40% yield. Elemental analysis for dried **1** (without the MeOH solvate): Calculated (%) for $C_{81}H_{69.5}N_6O_{12.5}Cl_{3.5}Mn_3$: C, 60.21; H, 4.34; N, 5.20; Found: C, 59.79; H, 4.31; N, 5.22.

$[Mn^{III}_3O(Ph\text{-}sao)_3(4Me\text{-}sbz)_3(EtOH)_3]_2(OH)(NO_3)$ (**2**)

$Mn(NO_3)_2\cdot 4H_2O$ (251 mg, 1 mmol), Ph-saoH_2 (213 mg, 1 mmol) and NEt_3 (101 mg, 1 mmol) in EtOH (25 ml) was allowed to stir for 45 min at room temperature. To the resulting dark green solution 4Me-sbz (196 mg, 1 mmol) was added followed by paper filtration. The solution was left undisturbed to slowly evaporate at room temperature. X-ray quality dark green crystals of **2** were obtained in 40% yield. Elemental analysis for **2**: Calculated (%) for $C_{87}H_{84.5}N_{6.5}O_{12}Mn_3$: C, 66.22; H, 5.40; N, 5.77; Found: C, 65.85; H, 5.15; N, 6.01.

$\{[Mn_3O(Et\text{-}sao)_3(4,4'\text{-}bpy)_2(MeOH)]ClO_4\cdot 1.5MeOH\cdot Et_2O\}_n$ (**3**·1.5MeOH·Et_2O)

$Mn(ClO_4)_2\cdot 6H_2O$ (362 mg, 1 mmol), Et-saoH_2 (165 mg, 1 mmol) and MeONa (54 mg, 1 mmol) in MeOH (25 ml) was allowed to stir for 1 h at room temperature. To the resulting dark green solution 4,4′-bpy (625 mg, 4 mmol) was added followed by paper filtration. The solution was diffused with diethyl ether. X-ray quality dark green crystals of (**3**·1.5MeOH·Et_2O) were obtained in 40% yield. Elemental analysis for dried **3** (without the solvates): Calculated (%) for $C_{48}H_{47}N_7O_{12}ClMn_3$: C, 51.74; H, 4.25; N, 8.80; Found: C, 51.59; H, 4.39; N, 9.18.

Acknowledgements

EKB would like to thank the EPSRC and Leverhulme Trust and G.S.P. is grateful to the Special Account for Research Grants (SARG) of the National and Kapodistrian University of Athens for partial support of this work.

Notes and references

1 C. B. Aakeroy, N. R. Champness and C. Janiak, *CrystEngComm*, 2010, **12**, 22, and references cited therein: (*a*) E. K. Brechin and L. Cronin, *Angew. Chem., Int. Ed.*, 2009, **48**, 6948, and references cited therein; (*b*) L. R. Macgillivray, G. S. Papaefstathiou, T. Friscic, T. D. Hamilton, D.-K. Bucar, Q. Chu, D. B. Varshney and I. G. Georgiev, *Acc. Chem. Res.*, 2008, **41**, 280, and references cited therein.

2 (*a*) C. Rovira and J. Veciana, *CrystEngComm*, 2009, **11**, 2031; (*b*) C. J. Kepert, *Aust. J. Chem.*, 2009, **62**, 1079; (*c*) K. S. Murray, *Aust. J. Chem.*, 2009, **62**, 1081.

3 (*a*) W. Wernsdorfer, N. Aliaga-Alcalde, D. N. Hendrickson and G. Christou, *Nature*, 2002, **416**, 406; (*b*) S. Hill, R. S. Edwards, N. Aliaga-Alcalde and G. Christou, *Science*, 2003, **302**, 1015; (*c*) H. Miyasaka, K. Nakata, L. Lecren, C. Coulon, Y. Nakazawa, T. Fujisaki, K. Sugiura, M. Yamashita and R. Clérac, *J. Am. Chem. Soc.*, 2006, **128**, 3770; (*d*) J. Yoo, W. Wernsdorfer, E.-C. Yang, M. Nakano, A. L. Rheingold and D. N. Hendrickson, *Inorg. Chem.*, 2005, **44**, 3377; (*e*) C. Boskovic, R. Bircher, P. L. W. Tregenna-Piggott, H. U. Güdel, C. Paulsen, W. Wernsdorfer, A.-L. Barra, E. Khatsko, A. Neels and H. Stoeckli-Evans, *J. Am. Chem. Soc.*, 2003, **125**, 14046; (*f*) L. Lecren, W. Wernsdorfer, Y.-G. Li, A. Vindigni, H. Miyasaka and R. Clerac, *J. Am. Chem. Soc.*, 2007, **129**, 5045; (*g*) G. Novitchi, W. Wernsdorfer, L. F. Chibotaru, J.-P. Costes, C. E. Anson and Annie K. Powell, *Angew. Chem., Int. Ed.*, 2009, **48**, 1614; (*h*) L. F. Jones, A. Prescimone, M. Evangelisti and E. K. Brechin, *Chem. Commun.*, 2009, 2023; (*i*) R. Inglis, L. F. Jones, K. Mason, A. Collins, S. A. Moggach, S. Parsons, S. P. Perlepes, W. Wernsdorfer and E. K. Brechin, *Chem.–Eur. J.*, 2008, **14**, 9117.

4 (*a*) C. C. Stoumpos, R. Inglis, G. Karotsis, L. F. Jones, A. Collins, S. Parsons, C. J. Milios, G. S. Papaefstathiou and E. K. Brechin, *Cryst. Growth Des.*, 2009, **9**, 24; (*b*) G. Karotsis, L. F. Jones, G. S. Papaefstathiou, A. Collins, S. Parsons, T. D. Nguyen, M. Evangelisti and E. K. Brechin, *Dalton Trans.*, 2008, 4917; (*c*) G. Karotsis, C. Stoumpos, A. Collins, F. White, S. Parsons, A. M. Z. Slawin, G. S. Papaefstathiou and E. K. Brechin, *Dalton Trans.*, 2009, 3388; (*d*) R. Inglis, G. S. Papaefstathiou, W. Wernsdorfer and Euan K. Brechin, *Aust. J. Chem.*, 2009, **62**, 1108; (*e*) A. D. Katsenis, R. Inglis, A. M. Z. Slawin, V. G. Kessler, E. K. Brechin and G. S. Papaefstathiou, *CrystEngComm*, 2009, **11**, 2117.

5 (*a*) C. J. Milios, R. Inglis, A. Vinslava, R. Bagai, W. Wernsdorfer, S. Parsons, S. P. Perlepes, G. Christou and E. K. Brechin, *J. Am. Chem. Soc.*, 2007, **129**, 12505; (*b*) C. J. Milios, A. Vinslava, S. Moggach, S. Parsons, W. Wernsdorfer, G. Christou, S. P. Perlepes and E. K. Brechin, *J. Am. Chem. Soc.*, 2007, **129**, 2754; (*c*) C. J. Milios, A. Vinslava, W. Wernsdorfer, A. Prescimone, P. A. Wood, S. Parsons, S. P. Perlepes, G. Christou and E. K. Brechin, *J. Am. Chem. Soc.*, 2007, **129**, 6547; (*d*) R. Inglis, L. F. Jones, C. J. Milios, S. Datta, A. Collins, S. Parsons, W. Wernsdorfer, S. Hill, S. P. Perlepes, S. Piligkos and E. K. Brechin, *Dalton Trans.*, 2009, 3403.

6 (*a*) R. Inglis, L. F. Jones, G. Karotsis, A. Collins, S. Parsons, S. P. Perlepes, W. Wernsdorfer and E. K. Brechin, *Chem. Commun.*, 2008, 5924; (*b*) C. J. Milios, R. Inglis, L. F. Jones, A. Prescimone, S. Parsons, W. Wernsdorfer and E. K. Brechin, *Dalton Trans.*, 2009, 2812; (*c*) R. Inglis, S. M. Taylor, L. F. Jones, G. S. Papaefstathiou, S. P. Perlepes, S. Datta, S. Hill, W. Wernsdorfer and E. K. Brechin, *Dalton Trans.*, 2009, 9157.

7 (*a*) P. J. Stang, *Chem.–Eur. J.*, 1998, **4**, 19; (*b*) S. R. Seidel and P. J. Stang, *Acc. Chem. Res.*, 2002, **35**, 972; (*c*) L. Zhao, B. H. Northrop and Peter J. Stang, *J. Am. Chem. Soc.*, 2008, **130**, 11886; (*d*) B. H. Northrop, H.-B. Yang and P. J. Stang, *Chem. Commun.*, 2008, 5896.

8 (*a*) S. J. Dalgarno, N. P. Power and J. L. Atwood, *Coord. Chem. Rev.*, 2008, **252**, 825; (*b*) M. Yoshizawa, J. K. Klosterman and M. Fujita, *Angew. Chem., Int. Ed.*, 2009, **48**, 3418; (*c*) T. D. Hamilton, G. S. Papaefstathiou, T. Friscic, D.-K. Bucar and L. R. MacGillivray, *J. Am. Chem. Soc.*, 2008, **130**, 14366 and references cited therein.

9 (*a*) S. T. Meally, G. Karotsis, E. K. Brechin, G. S. Papaefstathiou, P. W. Dunne, P. McArdlea and L. F. Jones, *CrystEngComm*, 2010, **12**, 59; (*b*) S. T. Meally, C. McDonald, G. Karotsis, G. S. Papaefstathiou, E. K. Brechin, P. W. Dunne, P. McArdle, N. P. Power and L. F. Jones, *Dalton Trans.*, 2010, **39**, 4809–4816, and references cited therein.

10 (*a*) L. Carlucci, G. Ciani and D. M. Proserpio, *Coord. Chem. Rev.*, 2003, **246**, 247; (*b*) S. T. Hyde, A.-K. Larsson, T. D. Matteo, S. Ramsden and V. Robins, *Aust. J. Chem.*, 2003, **56**, 981.

11 (*a*) S. R. Batten, *CrystEngComm*, 2001, **18**, 1; (*b*) S. R. Batten and R. Robson, *Angew. Chem., Int. Ed.*, 1998, **37**, 1460; (*c*)

I. A. Baburin, V. A. Blatov, L. Carlucci, G. Ciani and D. M. Proserpio, *J. Solid State Chem.*, 2005, **178**, 2452; (*d*) V. A. Blatov, L. Carlucci, G. Ciani and D. M. Proserpio, *CrystEngComm*, 2004, **6**, 378.
12 (*a*) L. Carlucci, G. Cianni and D. M. Proserpio, *CrystEngComm*, 2003, **5**, 269; (*b*) J.-P. Sauvage, *Acc. Chem. Res.*, 1998, **31**, 611; (*c*) F. M. Raymo and J. F. Stoddart, *Chem. Rev.*, 1999, **99**, 1643; (*d*) S. A. Nepogodiev and J. F. Stoddart, *Chem. Rev.*, 1998, **98**, 1959.
13 (*a*) E. C. Sañudo, T. Cauchy, E. Ruiz, R. H. Laye, O. Roubeau, S. T. Teat and G. Aromí, *Inorg. Chem.*, 2007, **46**, 9045; (*b*) M. J. Knapp, D. N. Hendrickson, V. A. Grillo, J. C. Bollinger and G. Christou, *Angew. Chem., Int. Ed. Engl.*, 1996, **35**, 1818.
14 O. Roubeau and R. Clérac, *Eur. J. Inorg. Chem.*, 2008, 4325.
15 J. J. Borras-Alemnar, J. M. Clemente-Juan, E. Coronado and B. S. Tsukerblat, *J. Comput. Chem.*, 2001, **22**, 985.
16 G. S. Papaefstathiou, T. Friscic and L. R. MacGillivray, *ACA Transactions*, 2004, **39**, 110.
17 C. Birnara, V. G. Kessler and G. S. Papaefstathiou, *Polyhedron*, 2009, **28**, 3291.
18 L. R. MacGillivray, J. L. Reid, J. A. Ripmeester and G. S. Papaefstathiou, *Ind. Eng. Chem. Res.*, 2002, **41**, 4494.

